A Model for the Solution Structure of the Rod Arrestin Tetramer

Susan M. Hanson,[1,7] Eric S. Dawson,[2,3] Derek J. Francis,[4] Ned Van Eps,[5] Candice S. Klug,[4] Wayne L. Hubbell,[5,*] Jens Meiler,[1,2,6,*] and Vsevolod V. Gurevich[1,*]

[1]Department of Pharmacology
[2]Center for Structural Biology
[3]Department of Biochemistry
Vanderbilt University, Nashville, TN 37232, USA
[4]Department of Biophysics, Medical College of Wisconsin, Milwaukee, WI 53226, USA
[5]Jules Stein Eye Institute and Department of Chemistry and Biochemistry, University of California, Los Angeles, Los Angeles, CA 90095, USA
[6]Department of Chemistry, Vanderbilt University, Nashville, TN 37232, USA
[7]Present address: Department of Physiology, University of Wisconsin–Madison, 601 Science Drive, Madison, WI 53711, USA
*Correspondence: hubbellw@jsei.ucla.edu (W.L.H.), jens.meiler@vanderbilt.edu (J.M.), vsevolod.gurevich@vanderbilt.edu (V.V.G.)

SUMMARY

Visual rod arrestin has the ability to self-associate at physiological concentrations. We previously demonstrated that only monomeric arrestin can bind the receptor and that the arrestin tetramer in solution differs from that in the crystal. We employed the Rosetta docking software to generate molecular models of the physiologically relevant solution tetramer based on the monomeric arrestin crystal structure. The resulting models were filtered using the Rosetta energy function, experimental intersubunit distances measured with DEER spectroscopy, and intersubunit contact sites identified by mutagenesis and site-directed spin labeling. This resulted in a unique model for subsequent evaluation. The validity of the model is strongly supported by model-directed crosslinking and targeted mutagenesis that yields arrestin variants deficient in self-association. The structure of the solution tetramer explains its inability to bind rhodopsin and paves the way for experimental studies of the physiological role of rod arrestin self-association.

INTRODUCTION

Arrestins are ubiquitous regulators of G protein-coupled receptor (GPCR) signaling. They play a key role in desensitization and in switching signaling to G protein-independent pathways via interactions with regulatory proteins such as ERK1/2, JNK3, and Mdm2 (Gurevich and Gurevich, 2003, 2006a; Lefkowitz and Shenoy, 2005). The binding of free arrestins to these partners affects their subcellular localization (Song et al., 2006, 2007) and redirects their activity to alternative substrates (Hanson et al., 2007a).

Mammals express four arrestin subtypes. The two subtypes restricted to photoreceptors, rod (arrestin1; visual arrestin) and cone (arrestin4; X-arrestin) arrestin, bind rhodopsin and cone opsins, respectively. The two nonvisual arrestins, arrestin2 (β-arrestin; β-arrestin1) and arrestin3 (β-arrestin2), are ubiquitously expressed and bind hundreds of GPCR subtypes. The monomeric structures of bovine rod arrestin, arrestin2, and salamander cone arrestin are remarkably similar (Han et al., 2001; Hirsch et al., 1999; Sutton et al., 2005), with differences limited to several loops in which similar variations were found in different crystal forms of the same protein (Han et al., 2001; Hirsch et al., 1999).

Biologically, rod arrestin is unique in that it is the only arrestin with high specificity for just one receptor, rhodopsin. The concentration of endogenous arrestin in rods exceeds 1 mM (Broekhuyse et al., 1985; Hanson et al., 2007b; Strissel et al., 2006), which is several orders of magnitude higher than that of any other subtype (Chan et al., 2007; Gurevich et al., 2004). It is also the only arrestin that invariably crystallizes as a tetramer (Granzin et al., 1998; Hirsch et al., 1999).

Our previous study of rod arrestin self-association in solution revealed that it cooperatively forms tetramers, with a lower K_D for the dimer-tetramer equilibrium ($K_{D\ tet}$, 7.5 μM) than for the monomer-dimer equilibrium ($K_{D\ dim}$, 37 μM; Hanson et al., 2007c). These constants are well within the physiological range, so that the majority of rod arrestin likely exists as tetramer in vivo. In rods, arrestin moves between compartments in a light-dependent manner (Broekhuyse et al., 1985). This movement is thought to contribute to light and dark adaptation (Arshavsky, 2003; Calvert et al., 2006), and is believed to involve high-affinity binding of arrestin to activated phosphorhodopsin in the outer segments in the light, and low-affinity interaction with microtubules in the inner segments in the dark (Nair et al., 2005). All forms of rod arrestin bind microtubules, but only monomeric arrestin binds light-activated rhodopsin (Hanson et al., 2007c), identifying the tetramer as a "storage" form.

We introduced a nitroxide spin label (R1) at selected sites in the arrestin molecule to map intersubunit contacts in the solution tetramer (Hanson et al., 2007c). The effects of R1 on self-association, concentration-dependent changes in R1 mobility, and direct intersubunit distance measurements were inconsistent with the topology of the crystal tetramer (Hanson et al., 2007c). Extensive structure-function and electron paramagnetic resonance (EPR) studies demonstrate that the crystal structure of the arrestin monomer reflects its conformation in solution under
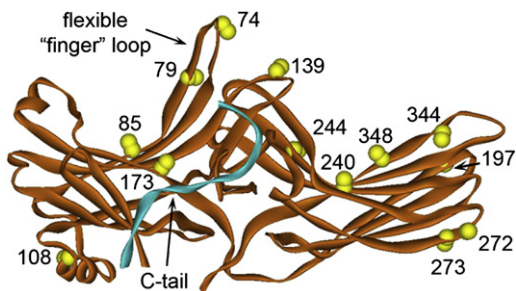
Figure 1. The Crystal Monomer and Location of Sites Studied
The 2.8 Å crystal structure of the visual arrestin monomer (PDB ID: 1CF1, chain A) (Hirsch et al., 1999) with the C-tail colored light blue and the sites used for modeling shown in yellow. Cα and Cβ carbons indicate the direction in which the side chain projects.

physiological conditions (Figure 1; Gurevich, 1998; Gurevich and Benovic, 1993; Gurevich and Gurevich, 2006b; Hanson et al., 2006b, 2007c). To unambiguously establish the biological function of rod arrestin self-association, it is critical to determine the structure of the solution tetramer and the specific intersubunit interfaces involved.

Here, we explore the topology of the rod arrestin tetramer in solution using computer modeling guided by experimental data. Protein-protein docking algorithms provide a means to elucidate structural details of unknown complexes. We used Rosetta (Gray et al., 2003a, 2003b; Schueler-Furman et al., 2005b; Wang et al., 2005), a recent method to predict protein-protein complexes from the coordinates of the free monomer components. The method employs a low-resolution, rigid-body Monte Carlo search followed by simultaneous optimization of backbone displacement and side-chain conformations. The resulting models are ranked using an energy function dominated by van der Waals interactions, an implicit solvation model, and an orientation-dependent hydrogen bonding potential. This method yielded a model of the arrestin tetramer in solution that accounts for the experimental data and is consistent with the cooperativity of its formation. Moreover, we demonstrate disulfide crosslinking predicted by the model and reveal that model-directed mutagenesis generates an arrestin variant with a significantly reduced propensity to self-associate.

RESULTS

Generation of a Solution Structure Model Using Protein-Protein Docking
To generate a molecular model of the solution tetramer we used restraints from light scattering, continuous wave (CW) EPR, and DEER experiments to guide protein-protein docking in Rosetta (Table 1; Hanson et al., 2007c). The residues used in the experimental restraints span the entire arrestin monomer (Figure 1).

First, 150,000 arrestin dimers were created by docking two copies of the monomer (1CF1, chain A) using the standard low-resolution Rosetta docking protocol (Gray et al., 2003a). Next, a low-resolution energy function with residue-level potentials (where side chains were replaced with centroid spheres) and the experimental intersubunit distances at residues 173 in

Table 1. Model Building and Evaluation Criteria

Residue	Located at an Intersubunit Interface?	Intersubunit Distances (Å)
V74		25–31, **34–38**, 43–50
F79	Yes	
F85	Yes	
Q89	No	
I108	No	49
V139		22–40
L173	Yes	25 and 49
F197	Yes	
L240		<18
V244	Yes	
S272	No	48
S273	No	33
S344		33
A348	Yes	

Criteria were derived from visible light-scattering and EPR spectroscopy data (interface residues) and DEER spectroscopy measurements (distances) as reported in Hanson et al. (2007c). Residues were designated to be at an intersubunit interface based on large reductions in self-association following introduction of the R1 spin label (sites 197, 244, 348) or concentration-dependent immobilization of R1 (sites 79, 85, 173). Distances (Å) are based on DEER spectroscopy measurements of arrestin spin labeled at the indicated site. For V74, the value shown in bold was given more weight in the restraint filter to account for the distance distribution pattern (see Figure 6D).

the N domain (25 Å) and 240 in the C domain (≤18 Å; Table 1; Hanson et al., 2007c) were used to filter these models to produce one set of 40 models having an N domain to N domain (NN) interaction and another 40 models with a C domain to C domain (CC) interface (Figure 2A). These 40 models of each dimer were subjected to a second round of standard low-resolution Rosetta docking (Gray et al., 2003a) to create tetrameric models. For this purpose each model was docked with a copy of itself, retaining symmetry at the dimer interfaces. Ten thousand models were created for each dimer, yielding 800,000 tetrameric structures. Based on the Rosetta energy score, the top 10% of these models were retained for further analysis (Figure 2B).

These 80,000 tetramers were filtered based on the experimental data using the following criteria:

(A) The cooperativity of tetramer formation (Hanson et al., 2007c; Imamoto et al., 2003) and the absence of higher-order oligomers (Imamoto et al., 2003) suggest that the solution tetramer has a closed symmetrical configuration. Therefore, each tetramer was given a symmetry score. Six distances can be measured between the four copies of one amino acid in a tetramer. In a symmetric tetramer, these six distances form three groups of two identical distances each. Symmetry was measured based on root mean squared deviations (rmsd; angstom units) from equidistance.
(B) The introduction of a spin label at sites 197, 244, and 348 produces large perturbations in arrestin self-association, suggesting that these sites are at or near a contact interface in the oligomer (Hanson et al., 2007c). Concentration-dependent
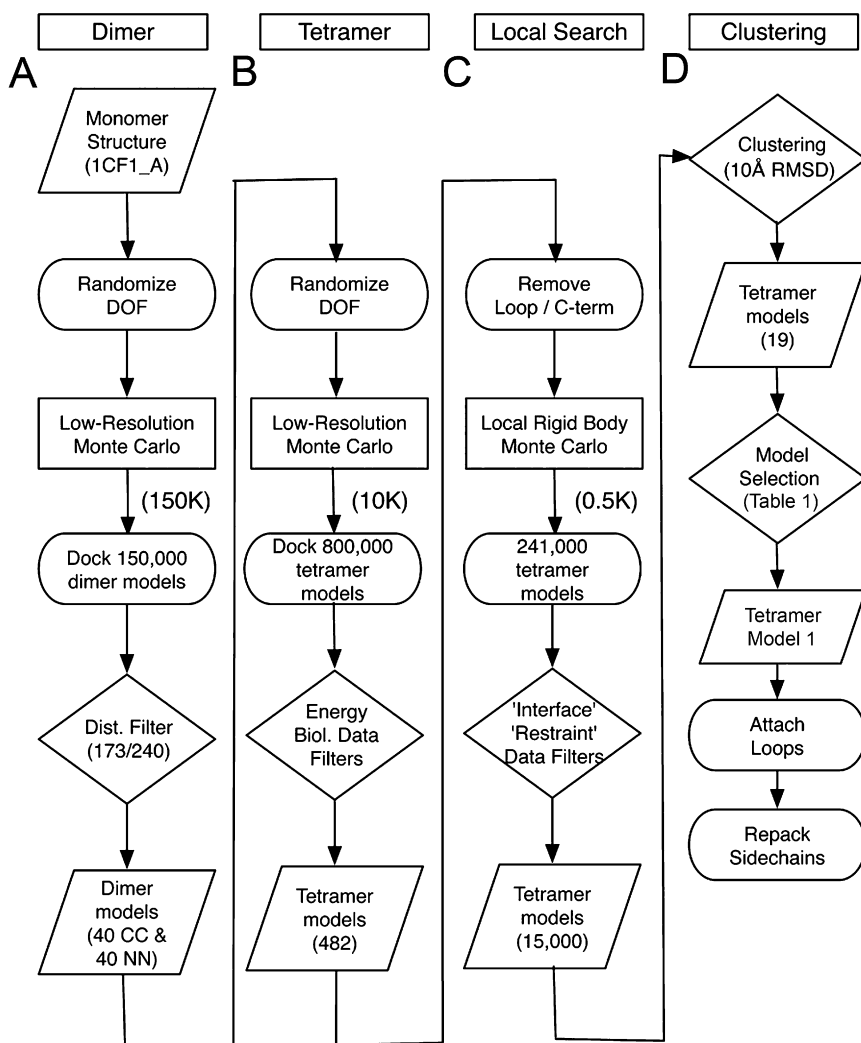
Figure 2. Flowchart of Molecular Modeling Steps

(A) Low-resolution global search and data filter for dimer model generation.

(B) Low-resolution global search and filters for tetramer model construction.

(C) Building procedure and higher-resolution local search for tetramer model refinement.

(D) Clustering for final model selection and refinement. Flowchart shapes indicate type of action performed: parallelogram (structure input/output); oval (model building operation); rectangle (conformational search algorithm); diamond (data filter or clustering decision point). DOF, degrees of freedom.

ous distance range, however imprecise, is sufficient to guide the protein docking calculations. No model was excluded based on violation of a single distance restraint, but models fitting multiple restraints were preferred. More precise methods that analyze spin label placement and movement explicitly are needed for analysis in less favorable cases (Borbat et al., 2002; Langen et al., 2000; Lietzow and Hubbell, 2004; Alexander et al., 2008).

Sorting of 80,000 tetramer models yielded 482 structures that passed all filters (Figure 2B). The nature of the global search space is shown in Figure 3A. To optimize the contact interfaces, the 482 best tetramer models were put through a local Monte Carlo minimization search, allowing translations of up to 10 Å and rotations of up to 30 degrees. Five hundred models per candidate tetramer (241,000 total) were generated (Figure 2C). The two most flexible regions, the loop containing residues 70–77 and the C terminus (residues 387–393) were removed at this stage to prevent misleading "clashes" near intersubunit interfaces. The 15,000 structures with the best combined scores for symmetry, interface, and restraint filters were clustered to arrive at 19 clusters with rmsd < 10 Å (Figure 2D).

changes in the EPR spectra of arrestin labeled at positions 79, 85, and 173 suggested that these sites also make direct contact with "sister" monomers (Table 1; Hanson et al., 2007c). This information was used to generate the interface filter, measuring the closest distance to these sites of an amino acid from a different monomer. If at least one other amino acid within 7 Å was found, the amino acid was assumed to be at an interface.

(C) The intermolecular distances between spin labels at seven sites (74, 139, 173, 240, 272, 273, and 344) determined by DEER spectroscopy (Table 1; Hanson et al., 2007c) were used to create a restraint filter. For this purpose, the experimentally observed distance between the spin labels was compared to an expected spin label distance based on α-carbon (CA) and β-carbon (CB) coordinates in the tetrameric models. A 7 Å vector was attached to the β-carbon, elongating the CA-CB vector. Its endpoint was assumed to represent the spin label. Distances between two of such endpoints were compared with the experimental distances. An error margin of 3 Å was added to the experimentally observed standard deviation to account for the imprecision of this simple model. This translation of a DEER distance into a gener-
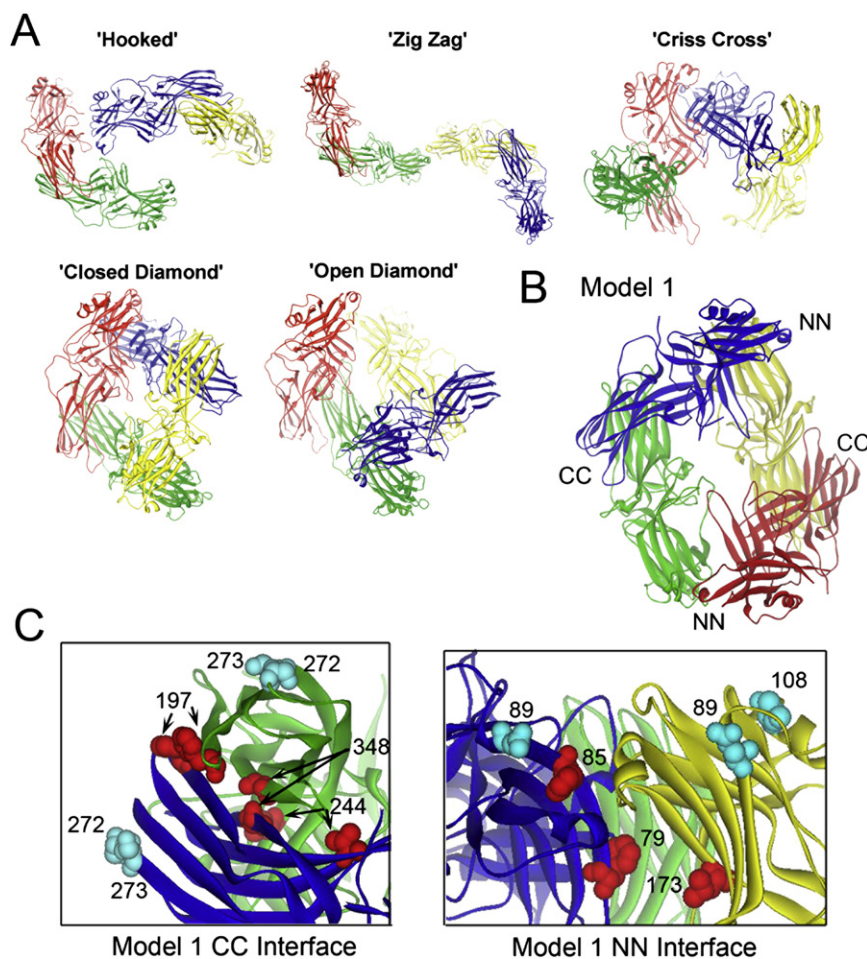
Representatives from each of these clusters were examined manually and either retained or eliminated based on the following criteria: (1) The structure must have a closed configuration that does not allow the formation of extended oligomers (Hanson et al., 2007c; Imamoto et al., 2003). (2) The structure must match (within 10 Å) all experimentally measured intersubunit distances (Table 1). (3) Residues in the model must be positioned in agreement with their known localization inside or outside intersubunit interfaces (Table 1).

This analysis identified a single best model (model 1; Figure 3B) for subsequent evaluation. Model 1 has a closed, diamond-shaped configuration with two nearly identical CC and NN interfaces. This model accounts for all distance measurements shown in Table 1 and is consistent with the positioning of

Figure 3. Representative Models of the Arrestin Tetramer

(A) Representative structures illustrating the breadth of search space covered in this study. Each tetramer is color coded by monomer.

(B) Model 1 is a representative structure from the largest cluster, which was identified as the best structural model of the solution tetramer based on the criteria in Table 1.

(C) A close-up view of model 1 showing the CC interface between two C domains (left) and the NN interface between two N domains (right). Residues shown to be located inside or outside contact interfaces (Hanson et al., 2007c) are highlighted in red and light blue, respectively.

233, 240, 267, and 344 show small concentration-dependent changes in mobility upon tetramer formation, but no evidence of strongly immobilized populations (Hanson et al., 2007c). For example, the EPR spectrum of 344R1 in the presence of excess wild-type (WT) arrestin reveals the appearance of a new dynamic state that reflects changes in the order of R1 motion without immobilization (Hanson et al., 2007c; Figure 4A). This suggests that these sites may be in the vicinity of interacting surfaces but not in direct contact. In model 1, each of these sites is located at or near an intersubunit interface (Figure 4B). Residue 344 is located at the CC interface but facing parallel to it, so that upon contact its motion would be dynamically altered without immobilization, in agreement with the data. In addition, spin labels at sites 89, 108, 272, and 273 show no motional changes in their EPR spectra upon tetramer formation (Hanson et al., 2007c), consistent with their locations outside of either the NN or CC interfaces in model 1 (Figure 3C). Thus, model 1 is consistent with the previously reported data (Hanson et al., 2007c).

residues known to be inside or outside contact interfaces (Hanson et al., 2007c; Figure 3C). Not only does model 1 stand out in its accordance to the experimental data, but it is a representative from the largest cluster, comprising 25% of the top 15,000 structures. The remaining clusters were discarded based on several violations of the evaluation criteria.

Of the top five clusters, none appear to show an intersubunit contact involving residue 173, even though significant concentration-dependent changes in spin-label mobility are observed for this residue (Hanson et al., 2007c). The observed changes of 173R1 mobility are likely due to intramolecular interactions. This residue is located near the NN interface in model 1, and it is possible that the C-tail of the same molecule (which rests next to it) comes into contact with 173 upon association with the adjacent monomer (Figure 1). Alternatively, repositioning of the flexible "finger" loop (70–77) upon self-association (Hanson et al., 2006b) may cause spin label immobilization at this site.

Model Is Consistent with Additional Spin Label Mobility Data

Much of the light scattering and EPR data from our initial study of the arrestin oligomer (Hanson et al., 2007c) were left out of the criteria used for modeling. Therefore, we used these additional data for initial tests of model 1. Spin labels at sites 72, 74, 139,

Experimental Testing of the Model: Mobility Changes at the NN Interface

To further test the validity of the NN interface in our model, we introduced a spin label either directly at the putative interface (residue 75) or outside it (residues 376 and 381; Figure 4C). The EPR spectra of 10 μM R1 arrestin with and without 180 μM WT arrestin (to promote tetramer formation) were compared to detect concentration-dependent changes in label mobility. The NN interface in the model yielded a reduction in mobility at position 75 and no significant changes at 376 or 381. The predicted changes in mobility at these locations were observed experimentally (Figure 4D). The spectrum of R1 at 75 shows broadening of the fast motional component and, most importantly, the appearance of a new immobilized population (Figure 4D, arrow); the two populations may be accounted for by rotamers of R1, one of which makes contact with the adjacent subunit, leading
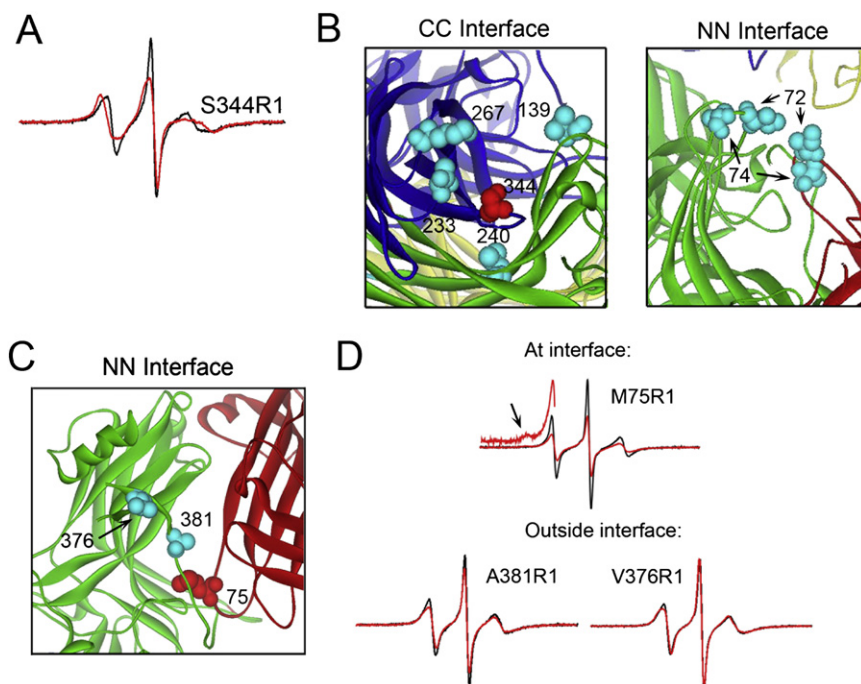
Figure 4. Concentration-Dependent Changes in the EPR Spectra of Spin-Labeled Arrestins Is Consistent with the Model
(A) The spectrum of 10 μM S344R1 in the absence (black trace) and presence of 180 μM WT arrestin (red trace).
(B) Close-up view of the CC and NN interfaces in model 1. Residues shown previously to be at or near a contact interface of the arrestin tetramer based on concentration-dependent changes in their EPR spectra (Hanson et al., 2007c) are shown in light blue and red (site 344).
(C) Close-up view of model 1 NN interface, depicting residues 75 (red), and 376 and 381 (light blue).
(D) For each site, the spectrum was recorded for 10 μM spin-labeled arrestin (black trace) and in the presence of 180 μM WT arrestin (red trace). For M75R1, the inset shows a magnified view of the low field region to more clearly reveal the immobilized component (arrow). The spectra are normalized to represent the same number of spins for each overlaid pair.

to immobilization. Much smaller changes in R1 mobility were observed at positions 376 and 381, with no evidence of an immobilized state. These results are consistent with the NN interface in model 1.

Experimental Testing of the Model: Disulfide Crosslinking

The residues Phe197 and Ala348 in the CC interface, and Thr157 and Asp162 in the NN interface in model 1, are close to their counterparts in the adjacent monomer (Figures 3C and 5B). In the crystal tetramer, all these residues are far from their counterparts (>20 Å). In contrast, residue Leu173 in the NN interface and Ser272 in the CC interface are far from their counterparts in model 1. To test these predictions, we created single cysteine mutants and determined their ability to form intersubunit disulfide bonds in solution.

In the presence of DTT, each arrestin ran as a single band on SDS-PAGE at a molecular weight (MW) corresponding to the arrestin monomer (+DTT) (Figure 5A). However, in the absence of DTT, the T157C, D162C, F197C, and A348C mutants showed a second band corresponding to the MW of the arrestin dimer (−DTT) (Figure 5A). This suggests that residues 157, 162, 197, and 348 are close enough to their counterparts in the arrestin oligomer to self-crosslink in solution. The absence of DTT for mutants L173C and S272C did not induce crosslinking, in agreement with their location in model 1 (Figure 5). These data strongly support the orientation of the NN and CC interfaces in model 1, because disulfide crosslinking occurs only when the Cβ-Cβ distance between two residues is close (~5 Å).

Enhanced Flexibility of C-Terminally Truncated Arrestin Disrupts Tetramer Formation

Eleven C-terminal amino acids are not resolved in the crystal monomer because of the flexibility of the C-tail. We removed an additional seven residues from the C-tail (387–393) during the high-resolution Monte Carlo minimization search to prevent misleading intersubunit clashes (Figure 2C). However, mutational analysis shows that the C-tail is an important element stabilizing the basal conformation of free arrestin (Gurevich, 1998; Gurevich and Benovic, 1992; Gurevich et al., 1994; Hirsch et al., 1999; Palczewski et al., 1994). Sedimentation equilibrium analysis showed that a truncated form of rod arrestin (2-368) had a ~4-fold reduction in its propensity to self-associate as compared with full-length protein (Schubert et al., 1999). These data suggest that the C-tail plays a direct or indirect role in oligomer formation.

To test this hypothesis, we used a form of truncated arrestin (Tr; 1-378) that has the same receptor-binding properties as 2-368 (Gurevich, 1998; Gurevich and Benovic, 1993; Schubert et al., 1999) and measured its average molecular weight at various concentrations using visible light scattering (Hanson et al., 2007c). Compared with WT arrestin (Figure 6A, red line), Tr arrestin has approximately one order of magnitude reduction in the overall propensity for tetramer formation (Figure 6A, black line; and Table 2). To test whether the disruption of self-association by truncation is a result of increased flexibility of the molecule (i.e., because intramolecular interactions holding it in its rigid basal conformation are destabilized), we performed intersubunit distance measurements of arrestin spin labeled at position 74 on the background of WT (V74R1) and the Tr form (V74R1Tr). If Tr arrestin is more flexible, the range of measured distances would be far greater for V74R1Tr than for WT V74R1.

First, we measured the equilibrium association of the two arrestins to ascertain that the spin label at position 74 was not detrimental to self-association. We found that 74R1 did not appreciably affect WT, and slightly enhanced self-association of Tr arrestin (Figure 6A). The equilibrium constants for both mutants indicated that they self-associate well enough to be used for
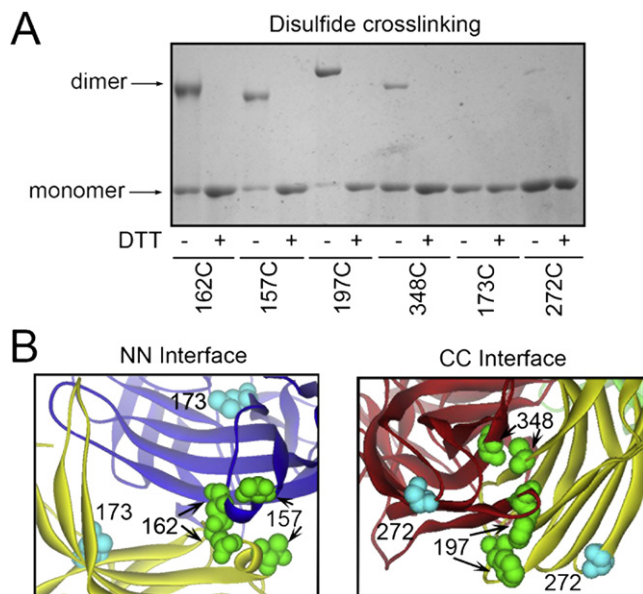
Figure 5. Residues in Close Proximity in the Model Form Disulfide Bonds

(A) Purified single cysteine mutants of arrestin in the presence (+) and absence (−) of 5 mM DTT were subjected to nonreducing SDS-PAGE and visualized by Coomassie staining as described in Methods. Molecular weight bands corresponding to arrestin dimer are present for 157C, 162C, 197C, and 348C in the absence of DTT. The apparent shift in molecular weight of the 197C dimer could be due to a difference in shape of the crosslinked species.

(B) Close-up view of the NN and CC interfaces of model 1 highlighting the sites used for disulfide crosslinking. Residues that do and do not self-crosslink are shown in green and light blue, respectively.

distance measurements (Table 2). Intermolecular distances between spin labels were then determined by DEER spectroscopy at 200 μM spin-labeled arrestin. The WT V74R1 distance distribution had a well-defined dominant population at ~35 Å, with minor populations at ≈28 Å and ≈48 Å (Figure 6B). In contrast,

V74R1Tr had a distance distribution spanning the entire range from ~20–55 Å (Figure 6B). Discrete populations within the distribution correspond approximately to those observed in WT V74R1, but the populations of the minor states have greatly increased.

The presence of a clear prevalent distance for WT V74R1 demonstrates that the motion of the flexible loop containing residue 74 is likely restricted by intersubunit contacts in the arrestin tetramer, and that the tetramer holds each arrestin monomer in a rigid conformation. The extremely broad range of distances of V74R1Tr shows that removal of the C-tail dramatically enhances the flexibility of this loop, either because truncation destabilizes intramolecular interactions holding arrestin in its basal conformation (Gurevich and Gurevich, 2004) or because the absence of the C-tail projecting across the cavity of the N domain (Figure 1) removes spatial constraints that inhibit the full range of motion of this loop. This is also supported by CW EPR spectra, which demonstrate that the mobility of V74R1Tr is higher compared with the full-length protein (Hanson et al., 2006b).

Collectively, the data suggest that truncated arrestin does not self-associate as well as WT because tetramer formation requires arrestin to be in a precise, somewhat inflexible conformation. The enhanced flexibility of the truncated form disturbs, but does not completely prevent, this process.

Targeted Disruption of Visual Arrestin Self-Association

To determine the functional role of rod arrestin self-association experimentally in vivo, one needs to dramatically alter tetramer formation by targeted mutagenesis without affecting other arrestin functions. Using model 1 (Figure 3B), we sought to create a rod arrestin mutant that does not self-associate at physiological concentrations. We combined some of the mutations that significantly disrupt tetramer formation (Hanson et al., 2007c) to create two doubly spin-labeled mutants. We found that the effect of spin label at two positions in the same domain (267 and 197 in the C domain; Figure 7A) did not exceed that of the more detrimental
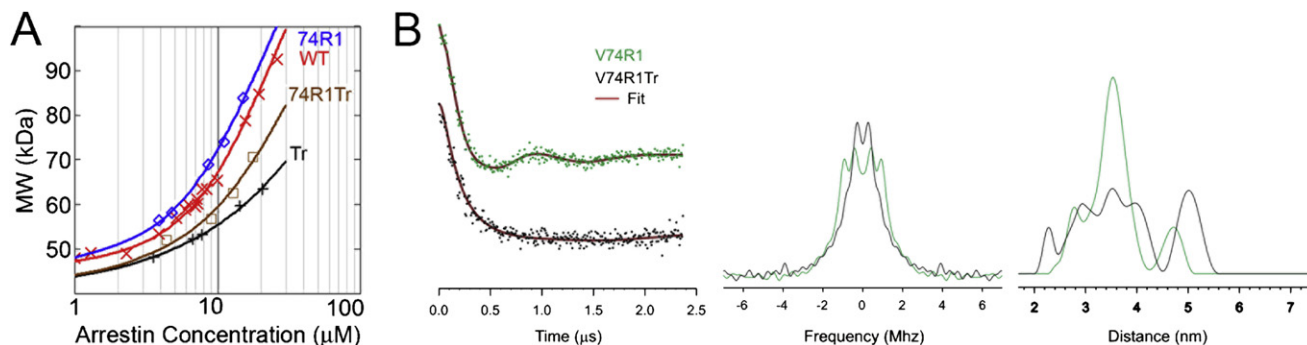

Figure 6. Removal of the C-Tail Enhances the Flexibility of the "Finger" Loop and Reduces Self-Association

(A) The average molecular weight of Tr (1-378) arrestin and V74R1 on the background of full-length (74R1) and truncated (74R1Tr) as a function of total arrestin concentration (symbols) were determined from the light-scattering data and fit to the MDT model (solid lines) as described (Hanson et al., 2007c). The WT arrestin data (red X) are shown for comparison.

(B) Internitroxide distance measurements of V74R1 on the background of full-length (green) and truncated (V74R1Tr) (black) arrestin by DEER spectroscopy. The DEER experiment measures the magnetic dipolar interaction between nitroxides as a modulation of the electron spin echo decay. The primary data is the echo amplitude as a function of time. The dipolar evolution function (left) is obtained after subtraction of an exponentially decaying background due to spins with randomly distributed interspin distances. Fourier transformation of the dipolar evolution function gives the Pake pattern (center). Fitting of the dipolar evolution function (left; red line) yields the experimental interspin distance distribution (right).

Table 2. Equilibrium Association Constants for WT and Spin-Labeled Arrestin Mutants

Arrestin	$\log K_1$ (log [M$_{-1}$])	$\log K_2$ (log [M$_{-1}$])	$\log K_o$ ($2*\log K_1 + \log K_2$)
WT	4.43 ± 0.02	5.13 ± 0.03	13.99 ± 0.07
Tr	4.45 ± 0.05	4.17 ± 0.18	13.07 ± 0.28
74R1	4.60 ± 0.05	5.09 ± 0.09	14.29 ± 0.19
74R1Tr	4.51 ± 0.07	4.70 ± 0.14	13.70 ± 0.28
85R1	4.30 ± 0.03		
197R1	3.89 ± 0.04		
267R1	4.30 ± 0.04		
197R1/267R1	3.83 ± 0.07		
85R1/197R1	3.34 ± 0.12		
85A/197A	3.28 ± 0.10		

The $\log_{10}$ of the dimer (K$_1$) and tetramer (K$_2$) equilibrium association constants (M^{-1}) and the overall association constant for tetramer formation (K$_o$ = K$_1^2$K$_2$) are shown. Constants were determined by least-squares fitting of the light-scattering data (Figures 6 and 7) as described (Hanson et al., 2007c). The oligomerization of 85R1, 197R1, and 267R1 was previously described by a monomer-dimer-tetramer equilibrium (Hanson et al., 2007c). For the weakly associating mutants the data can be just as well fit by a monomer-dimer equilibrium with the K$_1$ given.

197R1 alone (Figure 7B and Table 2). That the effects are not additive supports model 1, in which 267 and 197 are both in the same contact interface (Figure 7A). In contrast, the combination of 85R1 in the N domain with 197R1 in the C domain affects all four interfaces in our model (Figure 7A) and almost completely abolishes self-association (Figure 7C and Table 2). The additive effect fur-

ther corroborates the existence of separate NN and CC interfaces. To test whether removal of these specific residues per se or the introduction of the bulky spin label disrupts self-association, we replaced residues 85 and 197 with alanines. Double mutant 85A/197A has the same phenotype as the spin-labeled version (Figure 7C and Table 2), suggesting that the native phenylalanines in these positions are critical for tetramer formation because of specific interactions in their respective interfaces.

Taken together, our results demonstrate that model 1 (Figure 3B) reflects the structure of the physiologically relevant solution tetramer of rod arrestin and can be used as a guide for targeted disruption of its self-association.

DISCUSSION

Self-association of rod arrestin was discovered more than 20 years ago (Wacker et al., 1977), but attracted little attention until the arrestin crystal structure revealed similar tetramers crystallized under different conditions (Granzin et al., 1998; Hirsch et al., 1999). A follow-up study (Schubert et al., 1999) confirmed the formation of dimers and tetramers in solution and first proposed a hypothesis that arrestin oligomerization may regulate its activity in photoreceptors. This idea was based on the assumption that the arrestin oligomer is not a rhodopsin-binding species, although no direct functional comparison between monomers and oligomers was available at the time. Two subsequent small-angle X-ray scattering studies (Imamoto et al., 2003; Shilton et al., 2002) confirmed self-association but did not definitively determine the functional capabilities of rod arrestin
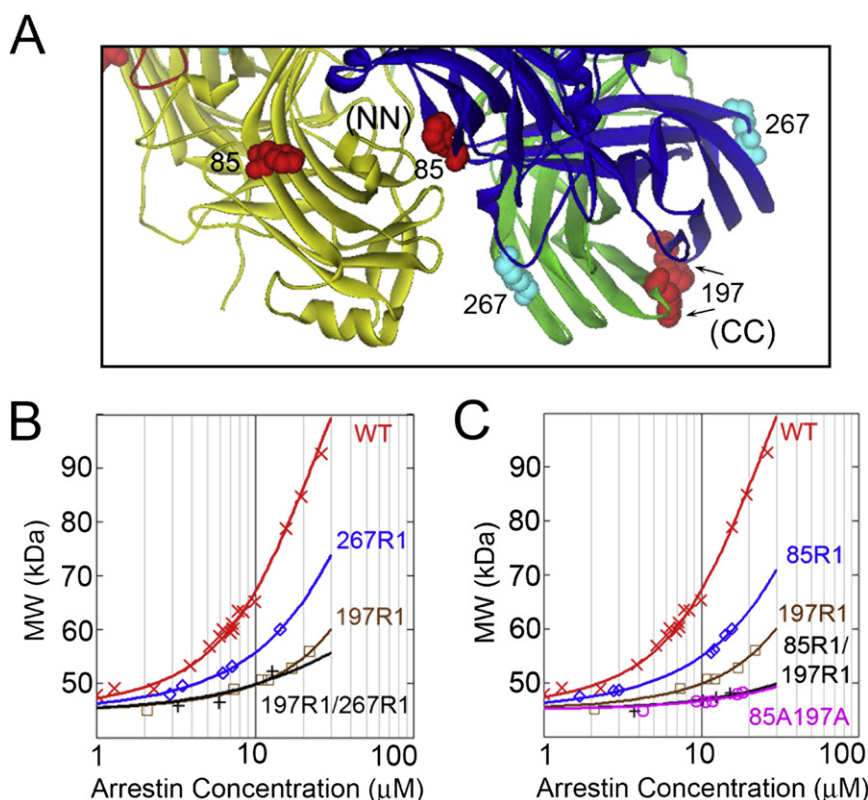
Figure 7. Targeted Disruption of Arrestin Self-Association

(A) Close-up view of model 1 depicting the CC and NN interfaces. Residues 197, 267 (CC), and 85 (NN) are highlighted.

(B and C) The average molecular weight of the indicated spin-labeled (R1) and alanine (A) arrestin mutants as a function of total arrestin concentration (symbols) were determined from the light-scattering data and fit to the MDT model (solid lines) as described (Hanson et al., 2007c). The WT arrestin data (red, X) are shown for comparison.

oligomers. A recent study using visible light scattering (Hanson et al., 2007c) confirmed the monomer-dimer-tetramer model proposed by Imamoto et al. (2003), where tetramer formation is cooperative (i.e., $K_{D\ tet} < K_{D\ dim}$) and determined the $K_{D\ tet}$ (7.5 μM) and $K_{D\ dim}$ (37 μM) with high precision.

The structure of the crystal tetramer does not account for the cooperativity of its formation: the contact area between monomers in the dimer exceeds that between dimers in the tetramer. Moreover, the open structure of the crystal tetramer suggests that further oligomerization could occur, which is not observed experimentally (Imamoto et al., 2003). The mapping of the inter-subunit interfaces using site-directed spin-labeling EPR and measurements of the intratetramer distances using DEER showed that the structure of the solution tetramer is dramatically different from that in the crystal (Hanson et al., 2007c). This study also demonstrated for the first time that though arrestin oligomers bind microtubules, only the arrestin monomer can bind rhodopsin (Hanson et al., 2007c). Therefore, the structure of the solution tetramer should explain the cooperativity of arrestin self-association, the absence of species larger than tetramer, and inability of oligomers to bind rhodopsin.

In recent years, docking algorithms have become substantially more reliable in predicting protein-protein complexes from the coordinates of the free components. In particular, RosettaDock (Gray et al., 2003a, 2003b; Schueler-Furman et al., 2005b; Wang et al., 2005) has performed superiorly in the critical assessment of predicted interactions (CAPRI) protein-protein docking experiment (Schueler-Furman et al., 2005a, 2005b; Wang et al., 2005). Protein-docking challenges in CAPRI typically do not include biological or structural information (other than the monomer starting coordinates) that would allow validation of the predicted models. Although no crystal structure of the biologically relevant arrestin tetramer is available, there is a wealth of complementary structural data. Though such data are usually believed insufficient to determine the structure of a protein complex, we show that when the experimental data provide multiple restraints, it can be sufficient to exclude alternative topologies predicted by Rosetta, leaving a single model.

The resulting diamond-shaped structure (model 1; Figure 3B) explains the cooperativity of tetramer formation, because the interaction between two dimers engages two interfaces, whereas dimerization involves only one. The circular closed configuration (Figure 3B) engages all the arrestin interfaces capable of binding sister monomers, thereby accounting for the absence of oligomers larger than a tetramer. Moreover, in every monomer the concave sides of the two arrestin domains that contain all of the identified receptor-binding elements (Gurevich and Benovic, 1993, 1995; Gurevich et al., 1995; Hanson et al., 2006b; Hanson and Gurevich, 2006; Ohguro et al., 1994; Pulvermuller et al., 2000; Vishnivetskiy et al., 2004) are either engaged in intersubunit interactions or shielded by other monomers (Figure 3B), providing the structural basis for the inability of the oligomer to bind the receptor.

Post hoc experimental tests, including spin label immobilization only at predicted interfaces (Figure 4), disulfide crosslinking only between predicted residues (Figure 5), and targeted disruption of self-association (Figure 7 and Table 2) add further support to the model. The solution tetramer has an extensive CC interface, suggesting that two monomers interacting via the C domains likely represent the solution dimer. This conclusion is supported by the tendency of spin labels in the C domain (e.g., positions 197, 233, 244, 267, 348) to primarily affect the dimerization constant, whereas spin labels in the N domain (e.g., positions 60, 72, 79) and the deletion of the C-tail primarily affect the tetramerization constant (Hanson et al., 2007c; Table 2). The C-tail projects across the N domain (Figure 1), stabilizing the basal state of the arrestin monomer (Gurevich, 1998; Gurevich and Benovic, 1992; Gurevich et al., 1994; Hirsch et al., 1999; Palczewski et al., 1994) and keeping the flexible "finger" loop in a specific orientation in the tetramer (Figure 6). Once removed, the C-tail, which is part of the NN interface (Figure 3B), can no longer participate in intersubunit contacts or intrasubunit interactions with the flexible loop. This disrupts the somewhat rigid conformation of arrestin required for tetramer formation, but has less of an effect on dimerization via the CC interface (Figure 3B). Collectively, these data strongly suggest that the CC intersubunit interaction represents the physiologically relevant solution dimer.

The microtubule-binding elements of monomeric rod arrestin and arrestin2 were mapped to the same concave surfaces of the molecule as those important for receptor binding (Hanson et al., 2006a, 2007a). However, microtubule binding does not affect the oligomeric state of arrestin (Hanson et al., 2007c), suggesting that monomer, dimer, and tetramer bind microtubules with similar affinity. Because the concave surfaces are largely shielded in the tetramer, there is likely an alternative microtubule-binding site on the non-receptor-binding side of the monomers within the CC dimer. Because separately expressed arrestin N domain is capable of binding microtubules (Hanson et al., 2006a, 2007a), we cannot exclude the possibility that the tips of "dangling" N domains in the CC dimer mediate its microtubule binding, and only the tetramer uses an alternative site on the non-receptor-binding surfaces of participating monomers. This issue needs to be resolved experimentally.

As was reported more than 20 years ago (Broekhuyse et al., 1985), and independently confirmed by two recent studies (Hanson et al., 2007b; Strissel et al., 2006), the amount of arrestin in rods is almost equimolar to rhodopsin (0.8:1). This translates into ~2.4 mM intracellular concentration; that is, approximately three to four orders of magnitude higher than any other arrestin in any other cell (Chan et al., 2007; Gurevich et al., 2004). We hypothesize that self-association is one of the mechanisms rods employ to keep this enormous amount of arrestin stored until it is needed to quench rhodopsin signaling (Gurevich et al., 2007; Hanson et al., 2007c). Most arrestin in the dark-adapted rod localizes to the inner segments, perinuclear area, and synaptic terminals (Broekhuyse et al., 1985; McGinnis et al., 2002; Mendez et al., 2003; Nair et al., 2005; Strissel et al., 2006)—cellular compartments particularly rich in microtubules (Eckmiller, 2000). Microtubule binding keeps the bulk of arrestin away from the rhodopsin-containing outer segment (Nair et al., 2005), with only 1%–7% of it residing in this compartment in the dark (Hanson et al., 2007b; Nair et al., 2005; Strissel et al., 2006). This translates into a total arrestin concentration of 24–168 μM in the dark-adapted outer segment. At first glance, this range appears to be large. However, if one takes into account that arrestin self-associates with $K_{D\ dim} = 37$ μM and $K_{D\ tet} = 7.5$ μM, the resulting concentration of monomer—the only active rhodopsin-binding arrestin species (Hanson et al., 2007c)—is kept within

a tight range: 11–23 μM. Thus, the combination of microtubule binding and self-association keeps a stable concentration of active arrestin monomer ready to quench rhodopsin signaling, while keeping an almost inexhaustible supply of stored arrestin available on demand (Gurevich et al., 2007).

Recent reports suggest that nonvisual arrestins may undergo assisted self-association in the presence of high physiological concentrations of inositol hexakisphosphate (IP6) (Milano et al., 2006). Quantitative analysis of this phenomenon under carefully controlled conditions shows that arrestin2 has little propensity to self-associate without IP6, but in the presence of 100 μM IP6 it cooperatively forms tetramers with a $K_{D\ dim}$ and $K_{D\ tet}$ similar to rod arrestin (Hanson et al., 2008). In contrast, IP6 inhibits self-association of rod arrestin (Hanson et al., 2008), suggesting that the shape of the rod and nonvisual arrestin tetramers may be different. The closest relative of the rod subtype, cone arrestin (Gurevich and Gurevich, 2006a), demonstrates virtually no self-association (Hanson et al., 2008). Apparently, its low expression level in cone photoreceptors (Chan et al., 2007) makes this storage mechanism unnecessary.

The ultimate test of the biological role of rod arrestin self-association requires the creation of mice expressing arrestin mutants with significantly decreased or enhanced propensity to self-associate while retaining normal ability to bind rhodopsin. The model of the physiologically relevant solution tetramer provides excellent guidance in this endeavor. The first attempts of model-based targeted disruption of arrestin self-association are encouraging.

EXPERIMENTAL PROCEDURES

Molecular Modeling
Arrestin tetramer models were assembled stepwise starting from the crystal structure coordinates for the arrestin monomer (1CF1, chain A) (Hirsch et al., 1999) using RosettaDock (Gray et al., 2003a) as described in the text and summarized in Figure 2. We adopted a conservative approach to modeling using the low-resolution scoring function of RosettaDock (see the Supplemental Data available online). An initial attempt at high-resolution refinement of each dimer interface produced wide-shaped binding funnels and predicted binding energies in a range comparable with the predicted binding energy for the crystal tetramer (1CF1) (Table S1). The entire model building and refinement process required ~150,000 CPU hours on Vanderbilt's Advanced Computing Center for Research and Education (ACCRE) high-performance computation cluster.

Site-Directed Mutagenesis and Arrestin Purification
Site-directed mutagenesis and arrestin expression and purification were performed as described (Gurevich and Benovic, 1995, 2000). All mutations were generated on the background of fully functional cysteine-less arrestin: ASA-CL (C63A, C128S, C143A) or VSV-CL (C63V, C128S, C143V) (Hanson et al., 2006a, 2006b).

Disulfide Crosslinking
Arrestin cysteine mutants (4–5 mg/ml) were dialyzed for >16 hr against two to three changes of 10 mM Tris (pH 8.5), 100 mM NaCl, 1 mM EDTA, and 1 mM EGTA buffer (−DTT) to induce disulfide bond formation. Five millimolars DTT was then added to a 10 μl aliquot of each sample and incubated for several hours (+DTT). A 1 μl aliquot of each sample, − and +DTT, was diluted in gel-loading buffer, subjected to 7.5% SDS-PAGE, and visualized with GelCode Blue Stain Reagent (Pierce, Rockford, IL).

Light Scattering
Light-scattering measurements were made with a DAWN EOS detector coupled to an Optilab refractometer (Wyatt Technology, Santa Barbara, CA) following gel filtration on a 7.8 mm (ID) × 15.0 cm (L) QC-PAK GFC 300 column (Tosoh Bioscience, Montgomeryville, PA). Experiments and calculations were carried out as described at length in (Hanson et al., 2007c).

EPR Spectroscopy
Arrestin cysteine mutants in 50 mM MOPS, 100 mM NaCl (pH 7.2) buffer were labeled with a 10-fold molar excess of 2,2,5,5-tetramethylpyrroline-3-yl-meth-anethiosulfonate spin label (MTSL) (Toronto Research Chemicals, North York, Ontario, Canada) overnight at 4°C, followed by removal of excess label as described (Hanson et al., 2006a, 2006b) to generate the R1 side chain. CW EPR spectroscopy was carried out at X band on a Bruker EleXsys 500 fitted with a super-high Q cavity. Samples (20 μl) were contained in a glass capillary, and spectra were recorded at room temperature over 100G at a microwave power of 10 mW and modulation amplitude of 1G, and were typically the average of 36–100 scans.

Four-Pulse DEER Measurements and Data Analysis
DEER measurements were performed using a Bruker EleXsys 580 spectrometer equipped with a 2 mm split-ring resonator at a temperature of 50 K as described (Hanson et al., 2007c). Echo decay data were analyzed using the DeerAnalysis2006 package (available at http://www.mpip-mainz.mpg.de/~jeschke/distance.html). Background echo decay was corrected using a homogeneous three-dimensional spin distribution. The distance distribution was calculated by fitting the corrected dipolar evolution data using Tichonov regularization as implemented in DeerAnalysis2006.

SUPPLEMENTAL DATA

Supplemental Data include Supplemental Experimental Procedures, one table, and one figure and can be found with this article online at http://www.structure.org/cgi/content/full/16/6/924/DC1/.

REFERENCES

Alexander, N., Al-Mestarihi, A., Bortolus, M., McHaourab, H., and Meiler, J. (2008). De novo high-resolution protein structure determination from sparse spin-labeling EPR data. Structure *16*, 181–195.

Arshavsky, V.Y. (2003). Protein translocation in photoreceptor light adaptation: a common theme in vertebrate and invertebrate vision. Sci. STKE. *204*, PE43.

Borbat, P.P., Mchaourab, H.S., and Freed, J.H. (2002). Protein structure determination using long-distance constraints from double-quantum coherence ESR: study of T4 lysozyme. J. Am. Chem. Soc. *124*, 5304–5314.

Broekhuyse, R.M., Tolhuizen, E.F., Janssen, A.P., and Winkens, H.J. (1985). Light induced shift and binding of S-antigen in retinal rods. Curr. Eye Res. *4*, 613–618.

Calvert, P.D., Strissel, K.J., Schiesser, W.E., Pugh, E.N., and Arshavsky, V.Y. (2006). Light-driven translocation of signaling proteins in vertebrate photoreceptors. Trends Cell Biol. *16*, 560–568.

Chan, S., Rubin, W.W., Mendez, A., Liu, X., Song, X., Hanson, S.M., Craft, C.M., Gurevich, V.V., Burns, M.E., and Chen, J. (2007). Functional

comparisons of visual arrestins in rod photoreceptors of transgenic mice. Invest. Ophthalmol. Vis. Sci. 48, 1968–1975.

Eckmiller, M.S. (2000). Microtubules in a rod-specific cytoskeleton associated with outer segment incisures. Vis. Neurosci. 17, 711–722.

Granzin, J., Wilden, U., Choe, H.W., Labahn, J., Krafft, B., and Buldt, G. (1998). X-ray crystal structure of arrestin from bovine rod outer segments. Nature 391, 918–921.

Gray, J.J., Moughon, S., Wang, C., Schueler-Furman, O., Kuhlman, B., Rohl, C.A., and Baker, D. (2003a). Protein–protein docking with simultaneous optimization of rigid-body displacement and side-chain conformations. J. Mol. Biol. 331, 281–299.

Gray, J.J., Moughon, S.E., Kortemme, T., Schueler-Furman, O., Misura, K.M., Morozov, A.V., and Baker, D. (2003b). Protein-protein docking predictions for the CAPRI experiment. Proteins 52, 118–122.

Gurevich, E.V., and Gurevich, V.V. (2006a). Arrestins are ubiquitous regulators of cellular signaling pathways. Genome Biol. 7, 236.

Gurevich, E.V., Benovic, J.L., and Gurevich, V.V. (2004). Arrestin2 expression selectively increases during neural differentiation. J. Neurochem. 91, 1404–1416.

Gurevich, V.V. (1998). The selectivity of visual arrestin for light-activated phosphorhodopsin is controlled by multiple nonredundant mechanisms. J. Biol. Chem. 273, 15501–15506.

Gurevich, V.V., and Benovic, J.L. (1992). Cell-free expression of visual arrestin. Truncation mutagenesis identifies multiple domains involved in rhodopsin interaction. J. Biol. Chem. 267, 21919–21923.

Gurevich, V.V., and Benovic, J.L. (1993). Visual arrestin interaction with rhodopsin: sequential multisite binding ensures strict selectivity towards light-activated phosphorylated rhodopsin. J. Biol. Chem. 268, 11628–11638.

Gurevich, V.V., and Benovic, J.L. (1995). Visual arrestin binding to rhodopsin: diverse functional roles of positively charged residues within the phosphorylation-recognition region of arrestin. J. Biol. Chem. 270, 6010–6016.

Gurevich, V.V., and Benovic, J.L. (2000). Arrestin: mutagenesis, expression, purification, and functional characterization. Methods Enzymol. 315, 422–437.

Gurevich, V.V., and Gurevich, E.V. (2003). The new face of active receptor bound arrestin attracts new partners. Structure 11, 1037–1042.

Gurevich, V.V., and Gurevich, E.V. (2004). The molecular acrobatics of arrestin activation. Trends Pharmacol. Sci. 25, 59–112.

Gurevich, V.V., and Gurevich, E.V. (2006b). The structural basis of arrestin-mediated regulation of G protein-coupled receptors. Pharmacol. Ther. 110, 465–502.

Gurevich, V.V., Chen, C.-Y., Kim, C.M., and Benovic, J.L. (1994). Visual arrestin binding to rhodopsin: intramolecular interaction between the basic N-terminus and acidic C-terminus of arrestin may regulate binding selectivity. J. Biol. Chem. 269, 8721–8727.

Gurevich, V.V., Dion, S.B., Onorato, J.J., Ptasienski, J., Kim, C.M., Sterne-Marr, R., Hosey, M.M., and Benovic, J.L. (1995). Arrestin interaction with G protein-coupled receptors. Direct binding studies of wild type and mutant arrestins with rhodopsin, β2-adrenergic, and m2 muscarinic cholinergic receptors. J. Biol. Chem. 270, 720–731.

Gurevich, V.V., Hanson, S.M., Gurevich, E.V., and Vishnivetskiy, S.A. (2007). How rod arrestin achieved perfection: regulation of its availability and binding selectivity. In Signal Transduction in the Retina, O. Kisselev and S.J. Fliesler, eds. (Boca Raton, FL: CRC Press), pp. 55–88.

Han, M., Gurevich, V.V., Vishnivetskiy, S.A., Sigler, P.B., and Schubert, C. (2001). Crystal structure of β-arrestin at 1.9 Å: possible mechanism of receptor binding and membrane translocation. Structure 9, 869–880.

Hanson, S.M., and Gurevich, V.V. (2006). The differential engagement of arrestin surface charges by the various functional forms of the receptor. J. Biol. Chem. 281, 3458–3462.

Hanson, S.M., Francis, D.J., Vishnivetskiy, S.A., Klug, C.S., and Gurevich, V.V. (2006a). Visual arrestin binding to microtubules involves a distinct conformational change. J. Biol. Chem. 281, 9765–9772.

Hanson, S.M., Francis, D.J., Vishnivetskiy, S.A., Kolobova, E.A., Hubbell, W.L., Klug, C.S., and Gurevich, V.V. (2006b). Differential interaction of spin labeled arrestin with inactive and active phosphorhodopsin. Proc. Natl. Acad. Sci. USA 103, 4900–4905.

Hanson, S.M., Cleghorn, W.M., Francis, D.J., Vishnivetskiy, S.A., Raman, D., Song, X., Nair, K.S., Slepak, V.Z., Klug, C.S., and Gurevich, V.V. (2007a). Arrestin mobilizes signaling proteins to the cytoskeleton and redirects their activity. J. Mol. Biol. 368, 375–387.

Hanson, S.M., Gurevich, E.V., Vishnivetskiy, S.A., Ahmed, M.R., Song, X., and Gurevich, V.V. (2007b). Each rhodopsin molecule binds its own arrestin. Proc. Natl. Acad. Sci. USA 104, 3125–3128.

Hanson, S.M., Van Eps, N., Francis, D.J., Altenbach, C., Vishnivetskiy, S.A., Arshavsky, V.Y., Klug, C.S., Hubbell, W.L., and Gurevich, V.V. (2007c). Structure and function of the visual arrestin oligomer. EMBO J. 26, 1726–1736.

Hanson, S.M., Vishnivetskiy, S.A., Hubbell, W.L., and Gurevich, V.V. (2008). Opposing effects of inositol hexakisphosphate on rod arrestin and arrestin2 self-association. Biochemistry 47, 1070–1075.

Hirsch, J.A., Schubert, C., Gurevich, V.V., and Sigler, P.B. (1999). The 2.8 Å crystal structure of visual arrestin: a model for arrestin's regulation. Cell 97, 257–269.

Imamoto, Y., Tamura, C., Kamikubo, H., and Kataoka, M. (2003). Concentration-dependent tetramerization of bovine visual arrestin. Biophys. J. 85, 1186–1195.

Langen, R., Oh, K.J., Cascio, D., and Hubbell, W.L. (2000). Crystal structures of spin labeled T4 lysozyme mutants: implications for the interpretation of EPR spectra in terms of structure. Biochemistry 39, 8396–8405.

Lefkowitz, R.J., and Shenoy, S.K. (2005). Transduction of receptor signals by β-arrestins. Science 308, 512–517.

Lietzow, M.A., and Hubbell, W.L. (2004). Motion of spin label side chains in cellular retinol-binding protein: correlation with structure and nearest-neighbor interactions in an antiparallel β-sheet. Biochemistry 43, 3137–3151.

McGinnis, J.F., Matsumoto, B., Whelan, J.P., and Cao, W. (2002). Cytoskeleton participation in subcellular trafficking of signal transduction proteins in rod photoreceptor cells. J. Neurosci. Res. 67, 290–297.

Mendez, A., Lem, J., Simon, M.I., and Chen, J. (2003). Light-dependent translocation of arrestin in the absence of rhodopsin phosphorylation and transducin signaling. J. Neurosci. 23, 3124–3129.

Milano, S.K., Kim, Y.-M., Stefano, F.P., Benovic, J.L., and Brenner, C. (2006). Nonvisual arrestin oligomerization and cellular localization are regulated by inositol hexakisphosphate binding. J. Biol. Chem. 281, 9812–9823.

Nair, K.S., Hanson, S.M., Mendez, A., Gurevich, E.V., Kennedy, M.J., Shestopalov, V.I., Vishnivetskiy, S.A., Chen, J., Hurley, J.B., Gurevich, V.V., et al. (2005). Light-dependent redistribution of arrestin in vertebrate rods is an energy-independent process governed by protein-protein interactions. Neuron 46, 555–567.

Ohguro, H., Palczewski, K., Walsh, K.A., and Johnson, R.S. (1994). Topographic study of arrestin using differential chemical modifications and hydrogen/deuterium exchange. Protein Sci. 3, 2428–2434.

Palczewski, K., Buczylko, J., Ohguro, H., Annan, R.S., Carr, S.A., Crabb, J.W., Kaplan, M.W., Johnson, R.S., and Walsh, K.A. (1994). Characterization of a truncated form of arrestin isolated from bovine rod outer segments. Protein Sci. 3, 314–324.

Pulvermuller, A., Schroder, K., Fischer, T., and Hofmann, K.P. (2000). Interactions of metarhodopsin II. Arrestin peptides compete with arrestin and transducin. J. Biol. Chem. 275, 37679–37685.

Schubert, C., Hirsch, J.A., Gurevich, V.V., Engelman, D.M., Sigler, P.B., and Fleming, K.G. (1999). Visual arrestin activity may be regulated by self-association. J. Biol. Chem. 274, 21186–21190.

Schueler-Furman, O., Wang, C., and Baker, D. (2005a). Progress in protein-protein docking: atomic resolution predictions in the CAPRI experiment using RosettaDock with an improved treatment of side-chain flexibility. Proteins 60, 187–194.

Schueler-Furman, O., Wang, C., Bradley, P., Misura, K., and Baker, D. (2005b). Progress in modeling of protein structures and interactions. Science *310*, 638–642.

Shilton, B.H., McDowell, J.H., Smith, W.C., and Hargrave, P.A. (2002). The solution structure and activation of visual arrestin studied by small-angle X-ray scattering. Eur. J. Biochem. *269*, 3801–3809.

Song, X., Raman, D., Gurevich, E.V., Vishnivetskiy, S.A., and Gurevich, V.V. (2006). Visual and both non-visual arrestins in their ''inactive'' conformation bind JNK3 and Mdm2 and relocalize them from the nucleus to the cytoplasm. J. Biol. Chem. *281*, 21491–21499.

Song, X., Gurevich, E.V., and Gurevich, V.V. (2007). Cone arrestin binding to JNK3 and Mdm2: conformational preference and localization of interaction sites. J. Neurochem. *103*, 1053–1062.

Strissel, K.J., Sokolov, M., Trieu, L.H., and Arshavsky, V.Y. (2006). Arrestin translocation is induced at a critical threshold of visual signaling and is super-stoichiometric to bleached rhodopsin. J. Neurosci. *26*, 1146–1153.

Sutton, R.B., Vishnivetskiy, S.A., Robert, J., Hanson, S.M., Raman, D., Knox, B.E., Kono, M., Navarro, J., and Gurevich, V.V. (2005). Crystal structure of cone arrestin at 2.3 Å: evolution of receptor specificity. J. Mol. Biol. *354*, 1069–1080.

Vishnivetskiy, S.A., Hosey, M.M., Benovic, J.L., and Gurevich, V.V. (2004). Mapping the arrestin-receptor interface: structural elements responsible for receptor specificity of arrestin proteins. J. Biol. Chem. *279*, 1262–1268.

Wacker, W.B., Donoso, L.A., Kalsow, C.M., Yankeelov, J.A., Jr., and Organisciak, D.T. (1977). Experimental allergic uveitis. Isolation, characterization, and localization of a soluble uveitopathogenic antigen from bovine retina. J. Immunol. *119*, 1949–1958.

Wang, C., Schueler-Furman, O., and Baker, D. (2005). Improved side-chain modeling for protein-protein docking. Protein Sci. *14*, 1328–1339.